Thermochimica Acta 554 (2013) 15–24

Contents lists available at SciVerse ScienceDirect

Thermochimica Acta

journal homepage: www.elsevier.com/locate/tca

Phase transformations of a talc ore under heated chlorine atmosphere

P. Orosco[a,*], M. del C. Ruiz[a,b], J. González[a,c]

[a] Instituto de Investigaciones en Tecnología Química (INTEQUI-CONICET), Chacabuco y Pedernera, 5700 San Luis, Argentina
[b] Facultad de Química, Bioquímica y Farmacia, Universidad Nacional de San Luis, Chacabuco y Pedernera, 5700 San Luis, Argentina
[c] Instituto de Ciencias Básicas, Universidad Nacional de Cuyo, Mendoza, Argentina

ARTICLE INFO

Article history:
Received 30 August 2012
Received in revised form 31 October 2012
Accepted 27 November 2012
Available online 19 December 2012

Keywords:
Talc
Protoenstatite
Thermogravimetry
Chlorination

ABSTRACT

The effect of Cl_2 on the phase transformations of the minerals present in a talc ($Mg_3Si_4O_{10}(OH)_2$) unpurified with clinochlore ($Mg_5Al_2Si_3O_{10}(OH)_8$), magnesite ($MgCO_3$), dolomite ($MgCa(CO_3)_2$), hematite (Fe_2O_3) and pyrite (FeS_2) was studied with the purpose of deferricating the mineral and obtaining protoenstatite ($MgSiO_3$), which is the basic component of steatite ceramics. Isothermal and non-isothermal assays in N_2 and Cl_2–N_2 atmospheres were performed using a thermogravimetric device at temperatures between 600 and 980 °C. The reagents and the products were analyzed by differential thermal analysis (DTA), X-ray diffraction (XRD), X-ray fluorescence (XRF), scanning electron microscopy (SEM), and electron probe microanalysis (EPMA). Results obtained showed that the following phenomena were produced in Cl_2: (a) The transformation of vitreous silica (SiO_2), from the chlorination reaction of talc, into enstatite ($MgSiO_3$) started at about 700 °C, being dolomite the mineral that favored this reaction. At 800 °C, more enstatite was formed as a result of the reaction between vitreous silica not transformed, $MgCl_2$ and O_2 derived from the chlorination of dolomite and magnesite; then, polymorphic transformation of enstatite into protoenstatite was produced. (b) At about 950 °C, $CaCl_2$ produced as a result of dolomite chlorination led to the destruction of the protoenstatite structure, and to the subsequent formation of cristobalite, with release of O_2 and gaseous $MgCl_2$. (c) The elimination of iron as $FeCl_3$(g) takes place in all the temperature interval investigated. The most favorable chlorination temperature was 900 °C, since protoenstatite structure was destroyed at higher temperatures and an efficient elimination of iron present in the talc sample was not possible at lower temperatures.

1. Introduction

Talc is a hydrated magnesium silicate with the formula $Mg_3Si_4O_{10}(OH)_2$, which belongs to the talc–pyrophyllite group, whose structure consists of a brucite octahedral sheet bonded to two silica tetrahedral sheets by oxygen atoms [1]. This mineral is widely used at industrial level due to its chemical inertia, softness, high thermal stability and low electrical conductivity [2]. An important technological application of talc is as the raw material from which steatite ceramics are obtained. The structure of the steatite ceramics is made up of approximately 70% magnesium metasilicate (protoenstatite phase), and 30% vitreous phase [3]. The protoenstatite is a high temperature polymorph of the enstatite. The initial composition of the mixture produced to obtain these materials has 80–90% talc; the rest of the mixture is made up of montmorillonite (and feldspar ($KAlSi_3O_8$), or barium carbonate ($BaCO_3$).

Steatite ceramics are ceramic-based materials used in electronics, electronic engineering and radio electronics due to their high mechanical resistance, low dielectric loss and temperature resistance [4,5]. The interest in steatite ceramics has increased over the last years due to their application as insulators in halogen lamps [6]. Furthermore, the use of this material in dental implants or crowns has also been investigated due to its high hardness and resistance to bending, as well as in bone implants, or coatings, due to its good biocompatibility [7,8].

The process of steatite ceramics thermal synthesis consists in the calcination of a mixture containing talc, montmorillonite (used as binding material), and feldspar, or barium carbonate (used as melting substance), at about 1400 °C, in order to produce the formation of a crystalline phase of magnesium metasilicate ($MgSiO_3$) from talc. Feldspar or barium carbonate forms a vitreous phase during the sinterization process, which melts and surrounds the crystalline phase [6,9].

The talc used in these ceramics must meet certain technical specifications, the most important one of which is iron content, because it affects the whiteness and the refractory properties of ceramics [10–12]. Another big problem affecting steatite ceramics is the formation of vitreous silica (SiO_2) during talc calcination, since its presence alters the dielectric properties of ceramics negatively [9,13].

* Corresponding author.
E-mail address: porosco@unsl.edu.ar (P. Orosco).

0040-6031/$ – see front matter © 2012 Elsevier B.V. All rights reserved.
http://dx.doi.org/10.1016/j.tca.2012.11.029

Table 1
Ores and minerals used.

Sample	Origin	Main minerals detected by XRD	Treatment
M1	Mendoza, Argentina	Talc, clinochlore, dolomite, magnesite	–
M2	Montana, United States	Talc, dolomite	–
M3	Mendoza, Argentina	Talc, clinochlore	M1 leaching with HCl
M4	Montana, United States	Talc	M2 leaching with HCl
M5	San Juan, Argentina	Dolomite, calcite	–
M6	Pure reactive, Sigma Aldrich	Hydromagnesite	–

Although studies referred to phase transformations during pure talc calcination in Cl_2 atmosphere [14] and talc deferrication by chlorination [12] have been conducted, there is no bibliographical data about phase transformations during the thermal treatment of talc ores in Cl_2 atmosphere.

In this work, the transformations undergone by talc ore thermally treated in a chlorine flow have been studied with a threefold purpose: first, obtaining protoenstatite (the main component of steatite ceramics) at a low temperature; second, improving the properties of this ceramic material by the elimination of impurities affecting it, and third, explaining the effect of the minerals commonly associated to talc during its chlorination mechanism.

2. Experimental

2.1. Materials

2.1.1. Ores and minerals

The samples used in this work, as well as their main characteristics and treatments, are described in Table 1.

The study was carried out using M1, a talc of ultramafic origin, containing the crystalline phases indicated in Table 1 and Fig. 1. Moreover, the sample contains pyrite and hematite, which were determined by scanning electron microscopy (SEM), and electron probe microanalysis (EPMA). SEM images of M1 sample are shown in Fig. 2. The particles marked with the symbols ◊ and ⬠ in Fig. 2a and b were analyzed by EPMA (Table 2). The composition of each particle suggests that they are hematite and pyrite particles.

T: theoretical composition corresponding to hematite (◊) and pyrite (⬠) formulas
E: experimental data

The amount of carbonate which form the M1 sample is 6.84% (w/w) magnesite, and 15.3% (w/w) dolomite.

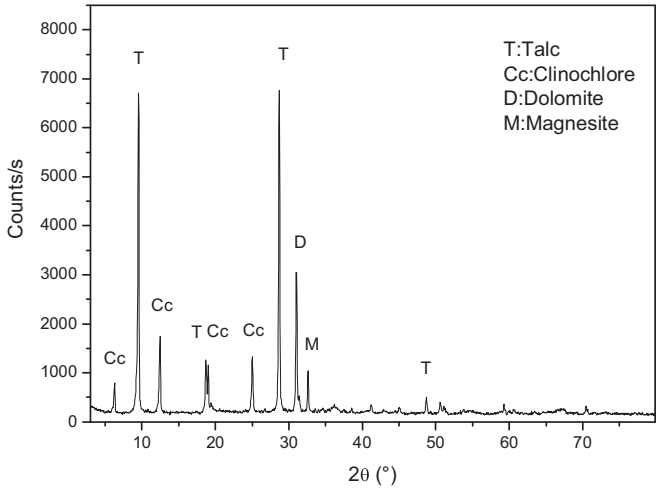

Fig. 1. XRD pattern of the M1 sample.

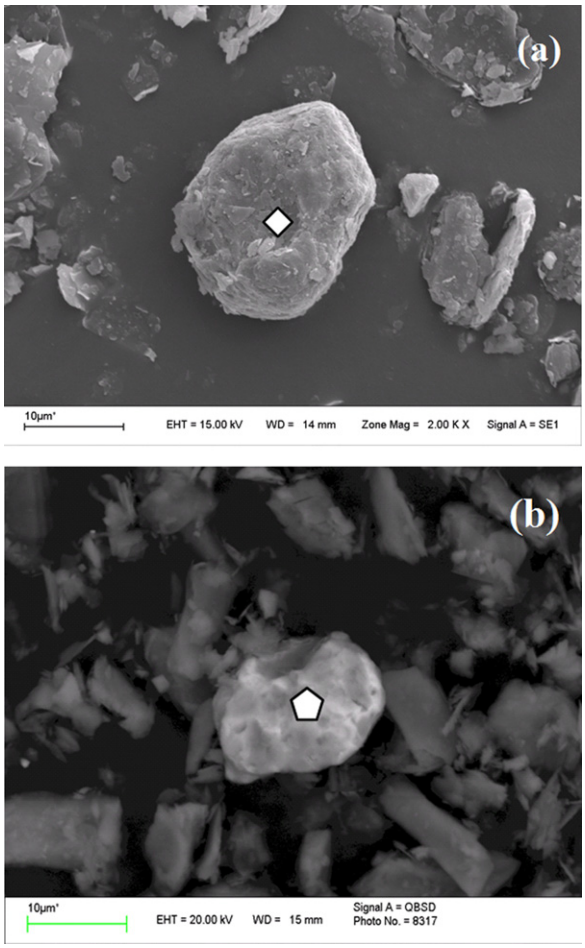

Fig. 2. SEM micrographs corresponding to minority particles of the M1 sample.

M2–M6 samples were used with the purpose of clarifying the effect impurities have on talc chlorination.

M1 and M2 were subjected to leaching with HCl in order to remove the carbonates present in both ores. The experimental procedure used was the following: each sample was leached with 10 wt.% HCl solution by softly shaking the suspension for 15 min. After that, the mixture was allowed to settle for 24 h. Once the solid residue was separated by decantation, it was recovered by filtering and washing it with hot distilled water. Finally, it was dried in a heater at 150 °C for a period of 30 min.

The solids resulting from the leaching process, called M3 and M4, do not contain magnesite and dolomite phases (Table 1).

2.1.2. Other reagents

The gasses used in the different assays were 99.5% chlorine, supplied by Cofil, Argentina, and 99.9% nitrogen, supplied by Air Liquide, Argentina. Hydrochloric acid was p.a. quality.

Table 2
EPMA analysis, in atomic %, corresponding to particles present in M1.

Particle	Mg		Al		Si		Fe		Ca		S		O	
	T	E	T	E	T	E	T	E	T	E	T	E	T	E
◊	–	–	–	–	–	–	69.94	65.16	–	–	–	–	30.06	34.84
⬠	–	–	–	–	–	–	46.55	47.23	–	–	53.45	52.77	–	–

2.2. Calcination procedure

Isothermal and non-isothermal calcination assays were carried out with a N_2 flow for trials in an inert atmosphere (N_2) and Cl_2/N_2 (50%) for chlorination assays, at a rate of 50 ml/min for both cases. These trials were performed on a thermogravimetric system designed to work in corrosive and non-corrosive atmospheres [15]. In each non-isothermal experiment, 1 g of sample was used, which was calcined in N_2 or Cl_2 flow at a heating rate of 5 °C/min until a temperature of 980 °C was reached. The mass change was recorded as a function of temperature. Isothermal experiments were also performed with 1 g of sample, which was placed inside the reactor and calcined in N_2 current at a heating rate of 10 °C/min, until the working temperature was reached. Once temperature was stable, Cl_2 was allowed to flow at 50% during a reaction time of 2 h. When the reaction time set for each assay was over, the flow of Cl_2 was interrupted, and the sample was purged with N_2 while the reactor cooled down. After completing the different isothermal calcination assays, the resulting solid residues were analyzed by XRD with a Rigaku D-Max-IIIC equipment, Cu Kα, operated at 35 kV, 30 mA.

The calcination of M1 was also performed under N_2 current using a Shimadzu differential thermal analyzer, at a heating rate of 5 °C/min, with the object of determining the phenomena that occur during calcination in an inert atmosphere.

3. Results and discussion

3.1. Calcination in N_2

Thermal treatment in N_2 on the different samples was performed with the purpose of having a reliable reference database, which made it possible to determine the phenomena attributable to the Cl_2 effect.

Data on calcination in air of minerals present in talc ore, which are provided by the bibliography, could help to explain the phenomena occurring during calcination in N_2.

Both the thermogram and the differential thermal analysis in N_2 of the talc M1 sample are presented in Fig. 3. The thermogravimetric curve obtained can be divided into four mass loss regions.

The first region of mass loss, between 50 and 100 °C, was the result of the elimination of water physically adsorbed in the sample. The dehydration process was observed in the DTA curve (Fig. 3) as an endothermic peak at 65 °C [1,16].

The mass loss, in the temperature range from 550 to 650 °C, was fast, and corresponds to magnesite thermal decomposition, as well as to the dehydroxylation of the brucite sheet localized in the interlayer space of the clinochlore. The decomposition of magnesite produced a peak at 580 °C and the partial dehydroxylation of the clinochlore, a shoulder at 600 °C in the DTA curve (Fig. 3) [17,18].

In the third region of mass loss, between 650 and 800 °C, a high mass loss rate could be observed due to dolomite thermal decomposition and to total clinochlore dehydroxylation, since the structural water of 2:1 layer (which was part of chlinoclore) started to be eliminated at this temperature. This could also be seen in the DTA curve as an endothermic shoulder at 650 °C for the decomposition of dolomite and a peak at 750 °C for total clinochlore dehydroxylation [18,19].

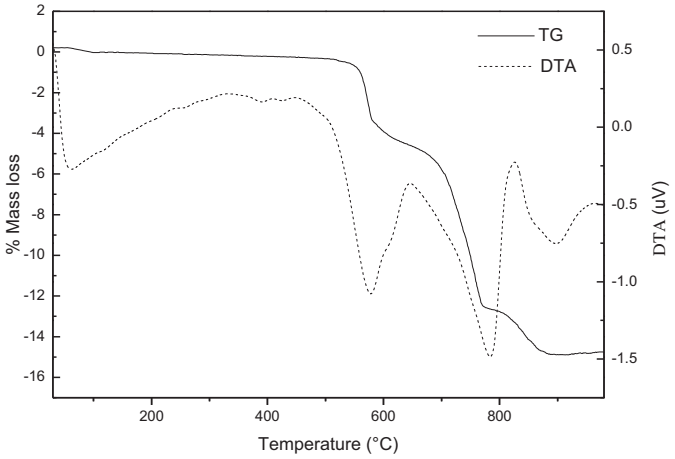

Fig. 3. TG and DTA curves of the M1 sample calcined in N_2.

The fourth zone of mass loss, in the temperature interval ranging from 750 to 900 °C, shows an endothermic peak at about 900 °C (Fig. 3), which corresponds to talc dehydroxylation. During this process, water elimination occurred together with a structure reordering caused by cations migration, which finally led to enstatite production, and to the formation of vitreous silica and water in form of vapor [16,20].

Thermogravimetric analyses were carried out on the samples M2–M6 in order to confirm those bibliographic data mentioned below, in relation to the mass changes observed in the different zones of Fig. 3, and to have reliable information on the phenomena that takes place during calcination of talc ore in N_2 atmosphere. XRD analyses were performed on the residues of these calcination assays. The experimental results are illustrated in Figs. 4 and 5 and discussed in the following sections.

3.1.1. First zone of mass loss (50–100 °C)

Talc dehydration can be experimentally proved by using the thermograms of M3 (M1 without carbonates) and M4 (M2 without carbonates) samples (Fig. 4b and d). The mass loss observed in these thermograms, between 50 and 100 °C, corresponds to the elimination of water physically adsorbed in the talc, which took place during calcination in N_2.

3.1.2. Second zone of mass loss (550–650 °C)

The phenomena produced in this region of mass loss can be elucidated with thermograms corresponding to M6 (hydromagnesite) and M3 samples (Fig. 4a and b), and with the XRD pattern of talc M1 calcined at 600 °C.

Three regions were visible in thermogram of Fig. 4a: the first two regions corresponded to the dehydration of intermediate products and carbon dioxide release, which generated magnesite [21]. The last stage of thermal decomposition, started at about 500 °C,

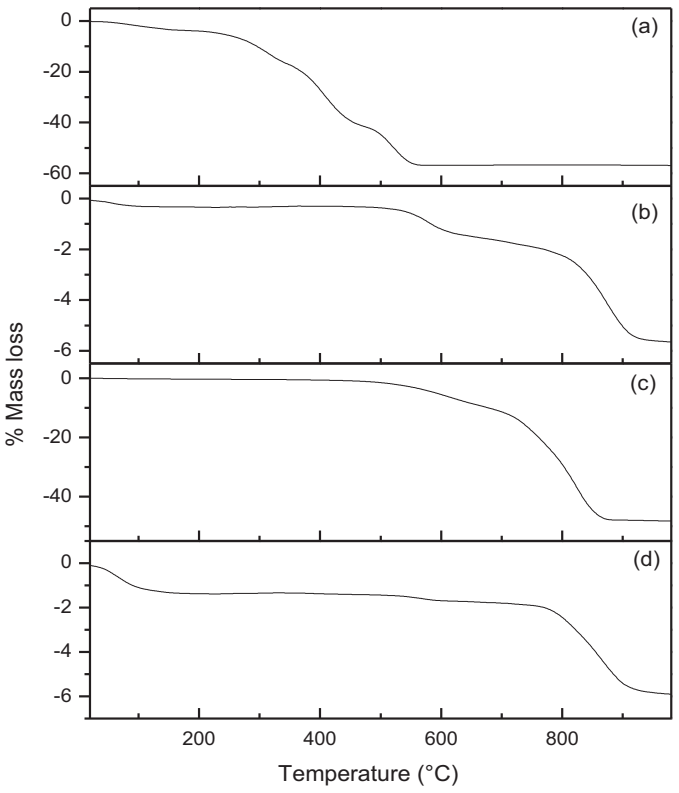

Fig. 4. Thermograms corresponding to different samples calcined in N_2: (a) M6, (b) M3, (c) M5 and (d) M4.

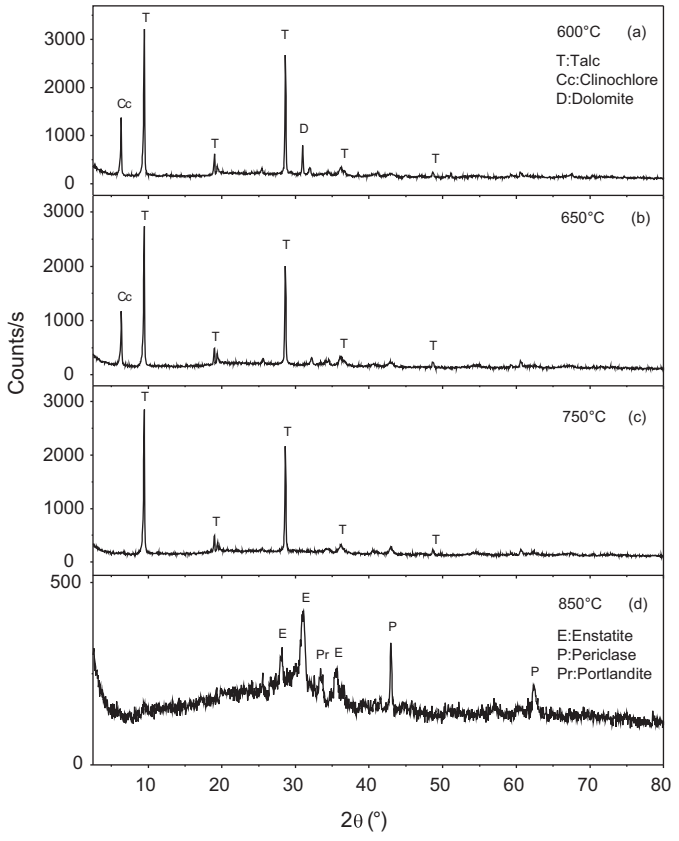

Fig. 5. XRD patterns of M1 sample calcined in N_2: (a) 600 °C, (b) 650 °C, (c) 750 °C and (d) 850 °C.

forming periclase (MgO) and carbon dioxide (CO_2) according to the reaction (1).

$$MgCO_3 \rightarrow MgO + CO_2(g) \quad (1)$$

The thermogram of M6 (Fig. 4a) indicated that magnesite was the mineral that decomposed at the lowest temperature during talc ore calcination.

Comparison of thermograms in Figs. 3 and 4a, as well as the observation of the fact that the magnesite phase in the original sample disappeared after calcinations at 600 °C (Fig. 5a), might suggest that magnesite thermal decomposition form part of the second region of mass loss observed in the thermogram of M1 (Fig. 3).

Clinochlore started decomposing at about 550 °C. This phenomenon could be observed as the first region of M3 mass loss (Fig. 4b), and in Fig. 5a as the disappearance of the 002, 003 and 004 reflections corresponding to the XRD pattern of M1 (2θ: 12.45°; 19.05° and 25.00°). This first clinochlore dehydroxylation, together with magnesite thermal decomposition, corresponded to the second region of M1 mass loss.

3.1.3. Third zone of mass loss (650–750 °C)

Thermograms of M3 and M5 (Fig. 4b and c), and XRD patterns of M1 calcined at 650 °C and 750 °C (Fig. 5b and c) allowed explaining the phenomena that occur in third zone of mass loss.

Total clinochlore dehydroxylation, which could be seen in Fig. 4b as slow mass loss of M3, started at about 650 °C and continued until 750 °C. At this temperature, the clinochlore phase disappeared from the calcination residue of M1 (Fig. 5c). This dehydroxylation process produced spinel ($MgAl_2O_4$), forsterite (Mg_2SiO_4), enstatite, and water according to reaction (2) and the result obtained by Villieras et al. [18] who works in the thermal treatment of clinochlore in similar conditions.

$$Mg_5Al_2Si_3O_{10}(OH)_8 \rightarrow MgAl_2O_4 + Mg_2SiO_4 + 2MgSiO_3 + 4H_2O(g) \quad (2)$$

Forsterite and spinel phases do not appear in the XRD pattern, probably because they are as amorphous phases.

Fig. 4c shows two stages of dolomite ore (M5) mass loss. The first one, at 500 °C, corresponded to the decomposition of the calcite ($CaCO_3$) accompanying dolomite. The second one started at about 700 °C, and corresponded to dolomite decomposition (reaction (3)), resulting in products like lime (CaO), periclase and carbon dioxide. Fig. 5b shows the disappearance of the dolomite phase when M1 was heated at 650 °C.

$$CaMg(CO_3)_2 \rightarrow CaO + MgO + 2CO_2(g) \quad (3)$$

3.1.4. Fourth zone of mass loss (750–900 °C)

Talc decomposition could experimentally be clarified by using the thermograms of M3 and M4 samples (Fig. 4b and d), as well as the XRD pattern of M1 calcined at 850 °C (Fig. 5d). This talc decomposition, which corresponded to the fourth region of M1 mass loss (Fig. 3), can be observed in Fig. 5d as the presence of the enstatite phase, according to reaction (4).

$$Mg_3Si_4O_{10}(OH)_2 \rightarrow 3MgSiO_3 + SiO_2 + H_2O(g) \quad (4)$$

Portlandite and periclase appeared at 850 °C due to the crystallization of oxides resulting from the thermal decomposition of carbonates (reaction (3)). The portlandite phase was produced by immediately hydrating lime after it was extracted from the reactor.

The analyses of M1, M3 and M4 thermograms (Figs. 3, 4b and d, respectively) suggest that talc dehydroxylation, which started at approximately 800 °C, continued until about 900 °C, since the mass of these samples remains constant at higher calcination temperatures.

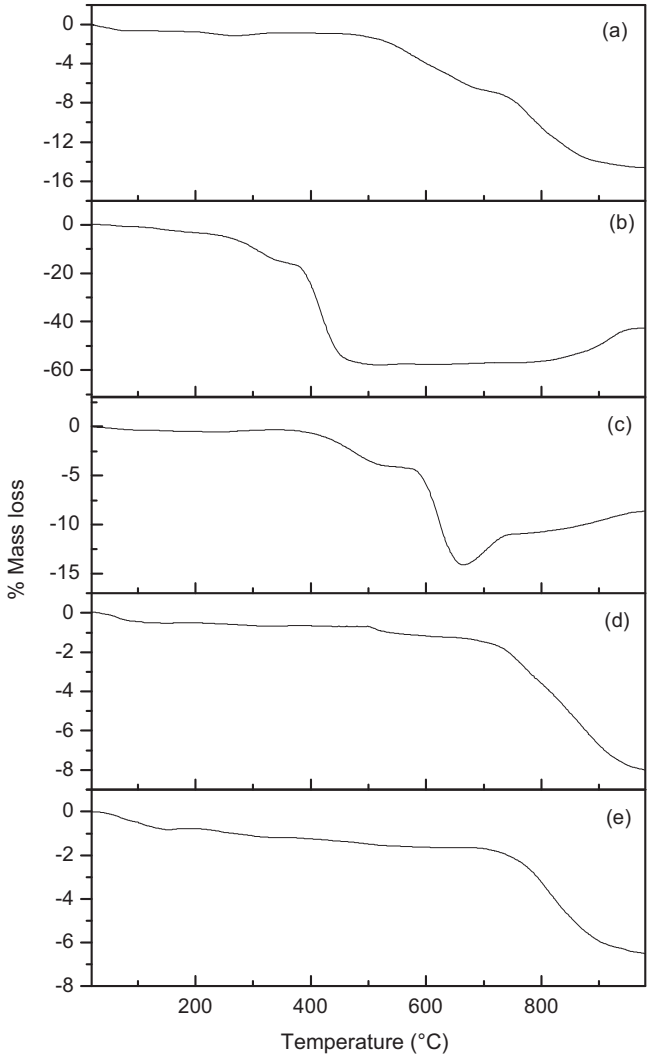

Fig. 6. Thermograms corresponding to different samples calcined in Cl_2: (a) M1, (b) M6, (c) M5, (d) M3 and (e) M4.

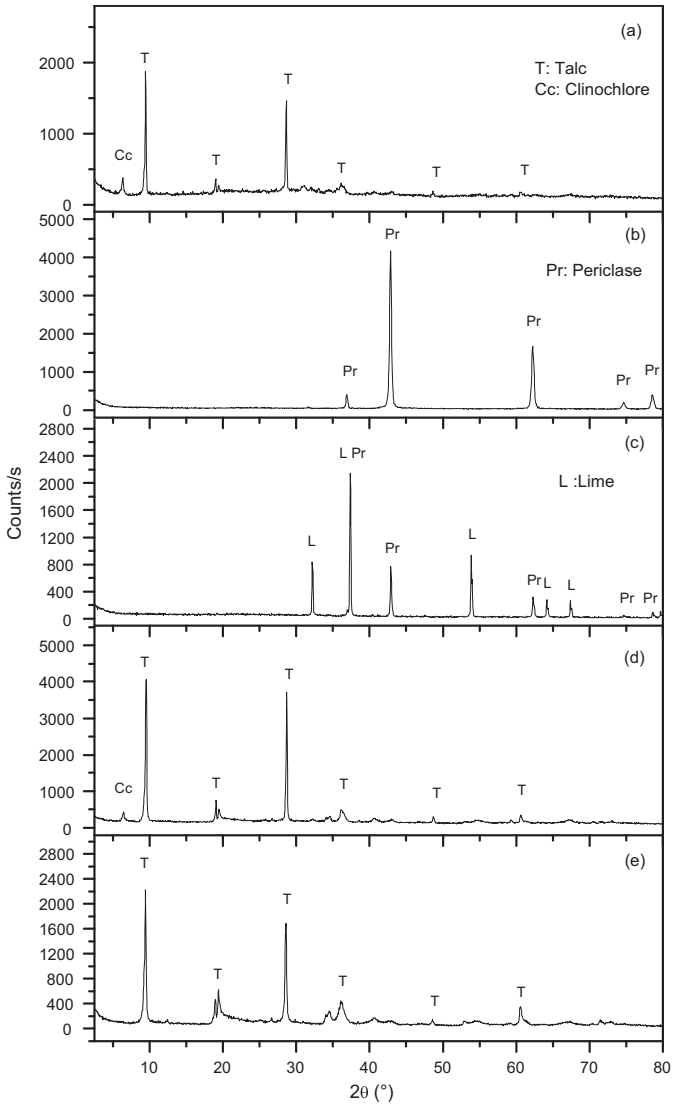

Fig. 7. XRD patterns corresponding to different samples calcined in Cl_2 at 600 ° C: (a) M1, (b) M6, (c) M5, (d) M3 and (e) M4.

3.2. Calcination in Cl_2

The thermogravimetric curve of M1calcination in Cl_2 (Fig. 6a) has three defined zones of mass loss. The first region could be observed in the temperature range between 450 and 700 °C; the second region could be seen between 700 and 900 °C, and the last region of mass loss, between 900 °C and the final temperature studied.

The thermograms of different samples used to determine the phenomena which took place during chlorination of M1 were also plotted in Fig. 6. The results of the XRD analysis performed on the residues of different chlorinated samples are presented in Figs. 7, 9, 10 and 13.

3.2.1. First zone of mass loss (450–700 °C)

The first region of mass loss started at 450 °C due to the reactions of magnesite and dolomite thermal decomposition. Halfway the first region of M1 mass loss, at about 550 °C, the dehydroxylation of interlayer brucite sheet of clinochlore was produced. This reactions can be clearly seen in the thermograms 6b–6d, corresponding to M6, M5 and M3 (hydromagnesite, dolomite and talc plus clinochlore, respectively).

Fig. 6b suggests that hydromagnesite thermal decomposition with carbon dioxide emission and formation of periclase took place at approximately between 400 and 450 °C. In the interval between 450 and 800 °C, no mass change is observed. Therefore, the XRD pattern of Fig. 7b proves the occurrence of the decomposition reaction of hydromagnesite, since the only phase present in it corresponds to periclase.

Thermogram in Fig. 6c shows two regions of mass loss corresponding to dolomite ore thermal decomposition that took place during chlorination. In the first region, periclase and calcite were formed with carbon dioxide emission; and in the second region, the mass loss was mainly produced as a consequence of lime formation and release of carbon dioxide.

The partial clinochlore dehydroxylation can be seen in Fig. 6d as the first zone of M3 mass loss, since this sample only contains talc and clinochlore (Fig. 6d), and in the XRD pattern of Fig. 7a and d, as the disappearance of the 002, 003 and 004 reflections of clinochlore (2θ: 12.45°, 19.05° and 25.00°).

On the other hand, the talc phase present in the samples M1, M3 and M4 was not observed to suffer any changes at 600 °C (Fig. 7a, d and e). These results indicated that chlorination did not affect talc structure at this temperature.

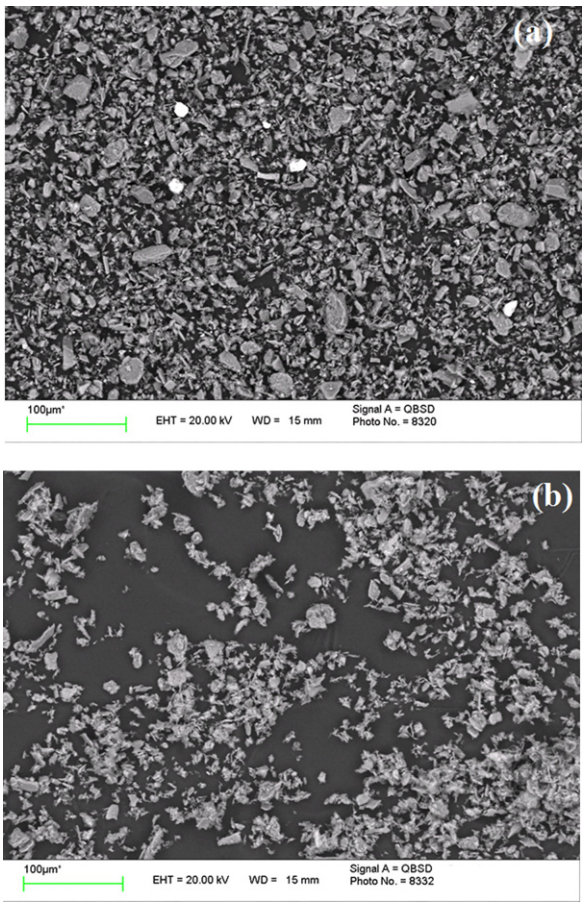

Fig. 8. SEM micrographs corresponding to M1 sample: (a) untreated, (b) calcined in Cl_2 at 600 °C.

Furthermore, in this temperature interval take places the chlorination of the pyrite [22] according to reaction (5).

$$FeS_2 + 5/2Cl_2(g) \rightarrow FeCl_3(g) + S_2Cl_2(g) \quad (5)$$

The results of the analysis realized by SEM and EPMA to the residues of chlorination at 600 °C probed the occurrence of the reaction (5). Fig. 8a and b show the images of SEM backscattered electrons corresponding to untreated M1 and M1 calcined in Cl_2 at 600 °C, respectively. According to the microanalysis results, the bright particles in Fig. 8a correspond to the pyrite phase. This phase is not observed in Fig. 8b.

3.2.2. Second zone of mass loss (700–900 °C)

The second region of talc M1 mass loss started at about 700 °C (Fig. 6a), and the thermogram showed a mass loss rate higher than that observed in the previous zone. The phenomena that took place in this mass loss region can be explained using the thermograms of samples M3–M6 (Fig. 6) and the XRD pattern of residues calcined at 700 and 800 °C in a Cl_2 atmosphere (Figs. 9 and 10).

The results of the analysis performed by XRD allowed inferring that the following reactions took place in this mass loss region:

$$(i)MgCa(CO_3)_2 + Cl_2(g) \rightarrow MgO + CaCl_2 + 2CO_2(g) + 1/2O_2(g) \quad (6)$$

$$(ii)1/3Fe_2O_3 + Cl_2(g) \rightarrow 2/3FeCl_3 + 1/2O_2(g) \quad (7)$$

$$(iii)1/2Mg_3Si_4O_{10}(OH)_2 + Cl_2(g) \rightarrow MgCl_2(l) + 1/2MgSiO_3 + 1/2O_2(g) + 1/2H_2O(g) + 3/2SiO_2 \quad (8)$$

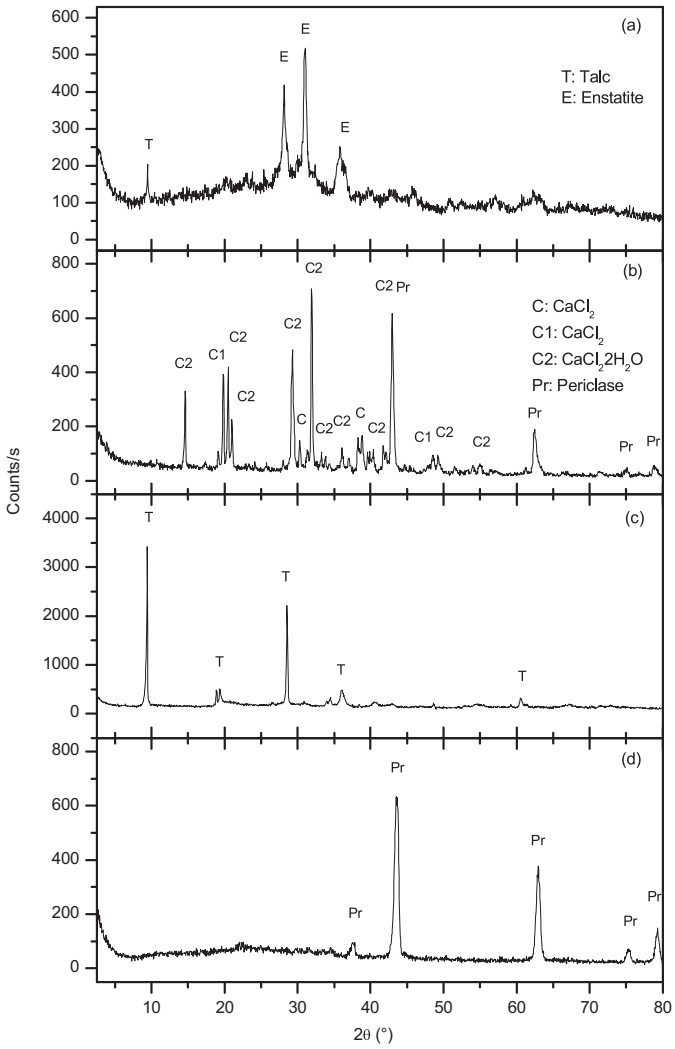

Fig. 9. XRD patterns corresponding to different samples calcined in Cl_2 at 700 °C: (a) M1, (b) M5, (c) M3 and M6.

$$(iv)MgCl_2(l) + SiO_2 + 1/2O_2(g) \rightarrow MgSiO_3 + Cl_2(g) \quad (9)$$

$$(v)Mg_5Al_2Si_3O_{10}(OH)_8 + Cl_2(g) \rightarrow 3MgSiO_3 + MgCl_2(l) + 4H_2O(g) + MgAl_2O_4 + 1/2O_2(g) \quad (10)$$

$$(vi)MgCa(CO_3)_2 + Cl_2(g) \rightarrow MgCl_2(l) + CaCl_2 + 2CO_2(g) + 1/2O_2(g) \quad (11)$$

$$(vii)MgCO_3 + Cl_2(g) \rightarrow MgCl_2(l) + CO_2(g) + 1/2O_2(g) \quad (12)$$

3.2.2.1. (i) Chemical interaction between dolomite and Cl_2 resulting in the formation of $CaCl_2$ (reaction (6)). The formation of the non-volatile $CaCl_2$ could be seen as a mass gain at approximately 700 °C (Fig. 6c). The XRD pattern of Fig. 9a indicated that the dolomite phase disappeared from the sample as a consequence of the interaction between this carbonate and chlorine, which led to the formation of calcium chloride and periclase at 700 °C, according to reaction (6). The occurrence of this reaction was probed by chlorinating a dolomite ore sample (M5) at the same temperature. The XRD pattern belonging to reaction (6) solid products, anhydrous calcium chloride and periclase are shown in Fig. 9b. Hydrated

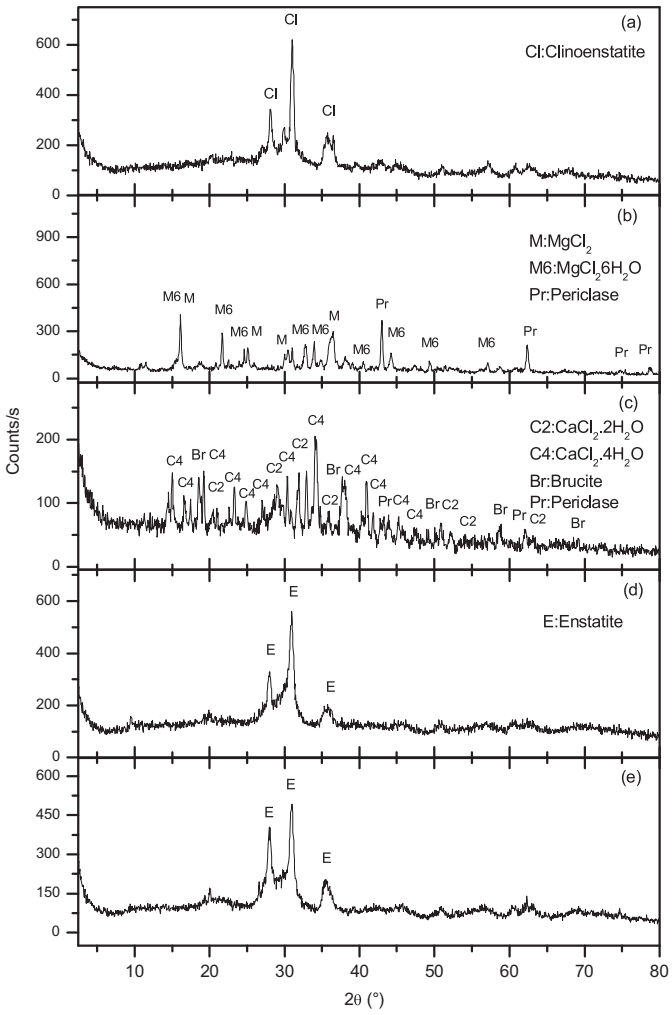

Fig. 10. XRD patterns corresponding to different samples calcined in Cl_2 at 800 °C: (a) M1, (b) M6, (c) M5, (d) M3 and (e) M4.

calcium chlorides were produced because the chlorination residue immediately hydrated after it was extracted from the reactor. At 800 °C, the periclase obtained from chlorination reacted with Cl_2 and produced $MgCl_2$. The variation in the mass increase observed from 800 °C in the thermogram, which corresponds to the dolomite ore (Fig. 6c), confirms the formation of $MgCl_2$.

3.2.2.2. (ii) Chlorination reactions of hematite present in the sample (reaction (7)). Hematite reacted with Cl_2 and produced $FeCl_3$ and O_2 [23–25]. Since these products are in gaseous state at 700 °C, they can be easily removed. The results of the analysis by XRF performed to the chlorination residues of M1 (Fig. 11) corroborate this phenomenon. According to the results obtained, hematite present in talc disappear at 700 °C due to the reaction between this mineral and Cl_2 (reaction (7)).

Fig. 11 shows the results of the iron analysis performed by XRF on the M1 sample residues which result from the treatment with chlorine at different temperatures and reaction times. It can be noted that a considerable increase in Fe_2O_3 extraction is produced in the temperature range between 600 and 700 °C. This is due to the fact that the iron that is being removed at this temperature interval is the most reactive one, such as the iron that is part of secondary minerals like pyrite and hematite, which is finely dispersed in talc [22,26].

The results of the analysis realized on chlorination residues by X-ray fluorescence show that the amount of iron removed by effect of

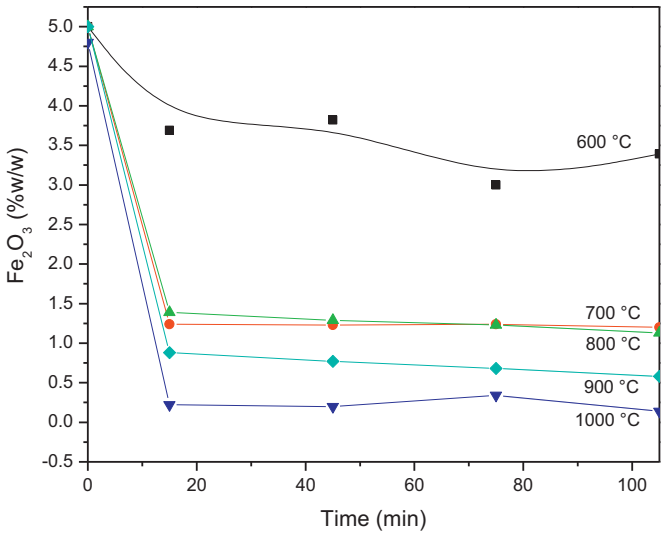

Fig. 11. Fe_2O_3 in residues of the M1 sample calcined in Cl_2.

chlorination at 600 °C, which corresponds to pyrite according to the results obtained by SEM and EPMA, is 1.3%, and the iron removed in the temperature interval between 600 and 700 °C, which corresponds to hematite and pyrite, is 3.75% (Fig. 11).

The balance between the amount of iron removed by hematite and pyrite chlorination, and the amount of iron in pyrite allows to estimate that the amount of iron corresponding to hematite is close to 2.45%.

3.2.2.3. (iii) and (iv) Cl_2 attack to talc structure with formation of enstatite (reactions (8) and (9)). By comparing the initial temperatures of the second mass loss region of the M1 chlorination (Fig. 6a) to the fourth region of mass loss corresponding to the calcination of the same sample in N_2 current (Fig. 3), we could infer that talc chlorination took place before thermal decomposition. The enstatite phase ($MgSiO_3$) observed in the XRD pattern of Fig. 9a indicated that talc reacted with Cl_2 at 700 °C, generating $MgCl_2$, enstatite and vitreous silica with oxygen and water release, according to the reactions (8) and (9).

Comparison between the XRD patterns corresponding to the chlorination of M1 residues (Fig. 9a) and carbonate-free talc, M3 (Fig. 9c), indicated that the presence of carbonates affected the formation of enstatite at 700 °C; and that $CaCl_2$ derived from dolomite chlorination was the reason why talc chlorination was produced at this temperature. The assumption on reactions (8) and (9) in relation to the $MgCl_2$ aggregation state was based upon the diagrams of Mg and Ca chloride phases [27], which indicate that the Mg and Ca chlorides form an eutectic mixture with a point of fusion of 620 °C. This liquid $MgCl_2$ later reacted with vitreous silica and oxygen liberated during chlorination, which generated enstatite, as indicated by reaction (9).

The occurrence of the reaction (9) has been experimentally verified. To this end, a calcination assay was carried out at 700 °C with a mixture of $MgCl_2$, $CaCl_2$ and vitreous silica at a 1:1:1 ratio, in a Cl_2–air (50%) flow, at a rate of 50 ml/min.

Fig. 12 shows the phases generated in the products of the mixture chlorination.

The experimental confirmation that reaction (9) actually takes place indicates that the reactivity of the species involved in it allows the reaction to be produced. The study of the mechanism by which this reaction is produced would be the object of another work.

The enstatite phase can be observed in this figure (JCPDS 86-433), which confirms the reaction between $MgCl_2$, SiO_2 and $O_2(g)$ producing this species.

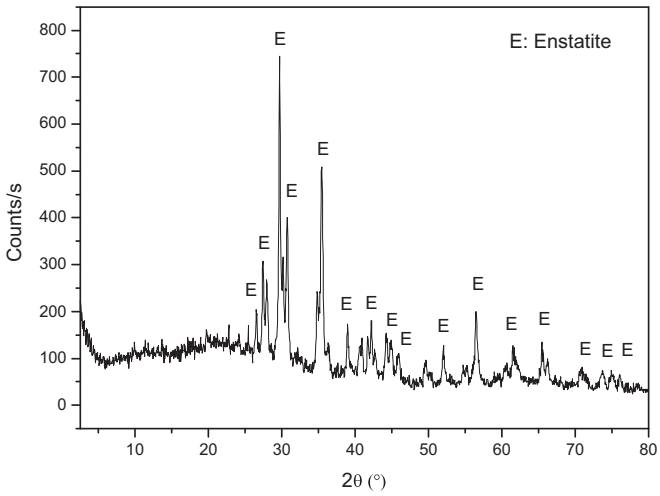

Fig. 12. XRD pattern corresponding to mixture $MgCl_2$–$CaCl_2$–SiO_2 calcined in Cl_2–air at 700 °C.

The experimental confirmation that reaction (9) actually takes place indicates that the reactivity of the species involved in it allows the reaction to be produced. The study of the mechanism by which this reaction is produced would be the object of another work.

3.2.2.4. (v) Clinochlore chlorination (reaction (10)). Clinochlore chlorination would yield enstatite, spinel, liquid $MgCl_2$, oxygen and water vapor at 700 °C, according to the reaction (10).

The XRD patterns of Fig. 9a and c show the disappearance of clinochlore 001 reflection (2θ, 6.23°); this phenomenon was not observed until 750 °C in inert atmospheres (Fig. 5c). The presence of $MgCl_2$ in liquid phase in reaction (10) was due to the formation of an eutectic mixture between $CaCl_2$ and $MgCl_2$.

3.2.2.5. (vii) and (viii) Enstatite and protoenstatite synthesis from carbonates and vitreous silica. The vitreous silica produced by reaction (8) of talc chlorination, which was not consumed by the reaction (9) of enstatite formation, reacted with the $MgCl_2$ produced by magnesite and dolomite chlorination [reactions (11) and (12)] at 800 °C, producing more enstatite.

On the other hand, enstatite obtained by all possible reactions was transformed into protoenstatite at 800 °C. This phenomenon, proved by the presence of the clinoenstatite phase in the XRD pattern (Fig. 10a), is due to the fact that clinoenstatite results as a consequence of the fast cooling of the protoenstatite phase, and that XRD analysis was performed at room temperature [6,13].

By comparing the XRD patterns corresponding to the chlorination of M1 (Fig. 10a) and M3 (Fig. 10d), we could infer that the presence of Ca and Mg carbonates affects the transformation of enstatite into protoenstatite. $MgCl_2$ obtained during talc ore chlorination could be responsible for the transformation of the phase observed at 800 °C because this chloride attacks the enstatite structure and generates an intermediate compound in liquid state, which in excess of Cl_2, crystallizes into protoenstatite afterwards.

3.2.3. Third zone of mass loss (900–980 °C)

The mass change produced in the zone of mass loss (Fig. 6a) is the result of two phenomena which are discussed below.

The first one is the increase of the $MgCl_2$ mass as a consequence of magnesite and dolomite chlorination (reactions (11) and (12)). The second is chlorination of the residue Fe_2O_3 remnant, which was occluded in the interlayer space of talc and iron, which was part of the clinochlore structure [12].

These phenomena are explained by the results of the analysis by XRF performed to the chlorination residues of M1 and TG and XRD analysis of M1–M6 samples.

$MgCl_2$ formation was detected in the thermograms corresponding to hydromagnesite (M6) and dolomite (M5) samples (Fig. 6b and c) as a mass gains which took place between 800 °C and the final temperature studied. The XRD pattern plotted in Fig. 10b shows the occurrence of $MgCl_2$ anhydrous and hydrated phases.

The data obtained by XRF on the removal of iron in the residues of M1 calcined between 800 and 1000 °C (Fig. 11) indicate that iron extraction shows little variation at 800 °C when compared to the one observed at 700 °C. These results can be attributed to the fact that the remaining iron is difficult to remove, since it is strongly adsorbed in the surface of minerals with laminar structure. A similar behavior has been observed during deferrication of clays [24,25], which need chlorination temperatures over 800 °C in order to reach a quantitative extraction of the iron present. It is therefore inferred that temperatures over 800 °C are necessary to extract this type of iron from talc.

The M1 mass loss observed between 900 °C and the final temperature investigated was produced as a consequence of the chlorination of the Fe_2O_3 occluded in the interlayer space of talc, and of that which was part of the clinochlore structure. This mass loss is also evidenced by the thermograms of M3 and M4 (Fig. 6d and e).

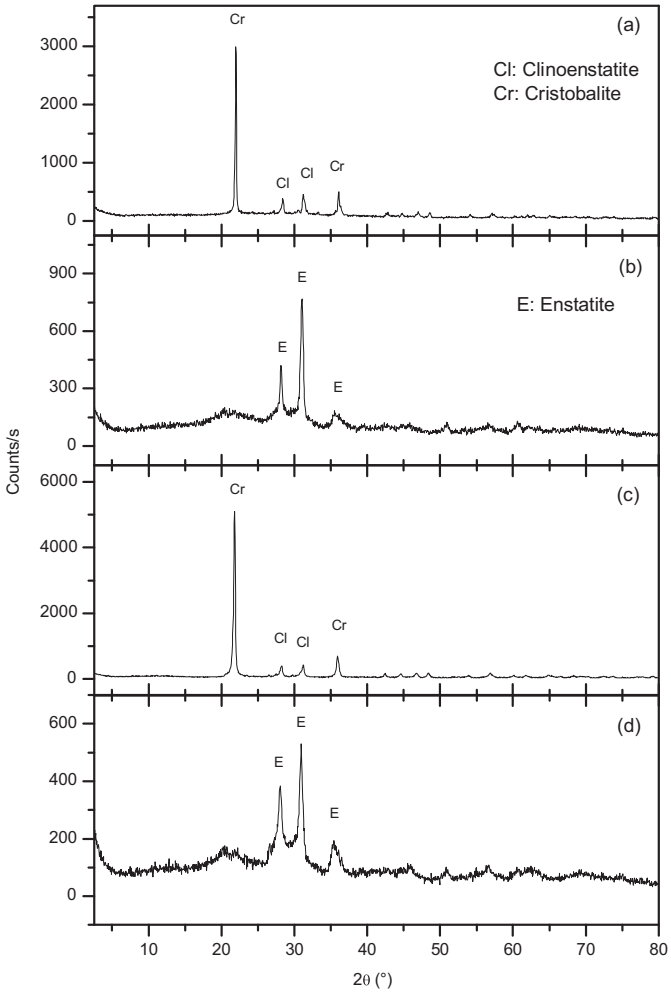

Fig. 13. XRD patterns corresponding to different samples calcined in Cl_2 at 1000 °C: (a) M1, (b) M3, (c) M2 and (d) M4.

Table 3
Mg content expressed as MgO in the calcination residues of M1 in Cl_2–N_2 atmosphere.

	Temperature (°C)				
	600	700	800	900	1000
MgO (%, w/w)	26.85	26.11	24.18	25.26	18.37

By comparing the XRD patterns of the M1 and M2 chlorination residues (Fig. 13a and c) to the residues of M3 and M4 (Fig. 13b and d), the effect of carbonates on the protoenstatite structure could be inferred. In these figures it is evident that the enstatite phase remains unaltered in the chlorination residues of carbonate-free leached samples, whereas the protoenstatite phase was attacked in minerals containing carbonates.

These experimental evidence allow us to say that partial protoenstatite chlorination was produced near the end of the third zone of mass loss (Fig. 6a), at approximately 950 °C, which resulted in products like crystoballite, gaseous $MgCl_2$, and oxygen, according to the following reaction:

$$MgSiO_3\,(\text{protoenstatite}) + Cl_2(g) \rightarrow SiO_2\,(\text{cristobalite}) + MgCl_2(g) + 1/2O_2(g) \quad (13)$$

$CaCl_2$ derived from dolomite chlorination was responsible for reaction (13), as it formed an eutectic mixture with the $MgCl_2$, which resulted in a higher volatilization of this chloride at 950 °C. Consequently, the chloride was removed from the reaction zone, favoring protoenstatite chlorination.

The chlorination of protoenstatite produces $MgCl_2$ at 950 °C according to reaction (13), and part of this $MgCl_2$ can volatilize since it has a vapor pressure of 0.0097 atm at this temperature [28]. Volatile $MgCl_2$ is removed from the reaction zone in the flow system used in this work, thus favoring the chlorination reaction of protoenstatite, and the formation of more volatile $MgCl_2$.

The chlorination reaction of protoenstatite has been experimentally proved by calcining the M1 sample at different temperatures for 120 min in a Cl_2–N_2 atmosphere, and then by determining the Mg content in the residues by XRF. Table 3 shows the result of these analyses.

The variation observed in the amount of Mg is the result of the balance between mass gain and loss of the sample as a consequence of the reactions that are produced by the effect of the thermal treatment of talc in Cl_2. A clear decrease of Mg content can be observed at 1000 °C. This is due to the volatilization of magnesium chloride, which takes place at around 950 °C.

By comparing the thermogravimetric curves described in Figs. 3 and 6a, we could observe that the mass loss continued until 980 °C, when the M1 sample was chlorinated, whereas the mass remained constant in N_2 current from 850 °C on. The behavior observed during the chlorination of M1 could also be detected during the chlorination of M3 (Fig. 6d), and this fact confirms that the removal of Fe_2O_3 in the form of $FeCl_3$, together with reaction (13), was produced.

4. Conclusions

(1) The results of the chlorination experimental assays proved that this process is an efficient method for obtaining protoenstatite (the main component of steatite ceramics) at low temperatures (800 °C). Moreover, chlorination has another advantage, which is reducing iron content that affects seriously the quality of this ceramic material.
(2) The study performed allowed determining the effects of carbonates on the chlorination process of talc and the mechanisms involved in the reactions produced.
(3) The enstatite was produced by the reactions of talc and clinochlore chlorination (reactions (8) and (10)), and it was also formed by the reaction between magnesium chloride, oxygen and vitreous silica, generated during the chlorination of talc ore (reaction (9)). This phenomenon caused the removal of vitreous silica, the main impurity that affects the dielectric properties of steatite ceramics.
(4) The most favorable chlorination temperature was 900 °C, since protoenstatite structure was destroyed at higher temperatures and the efficient elimination of iron present in the talc sample was not possible at lower temperatures.
(5) Iron present in talc ore in the form of pyrite and hematite are removed in the temperature interval between 600 and 700 °C. At approximately 900 °C iron that was occluded in the interlayer space, and that which was part of the clinochlore structure were also eliminated. Chlorination of this element continued until final investigated temperature was reached. According to these experimental results, chlorination is an effective method for removing iron from talc ore.
(6) Calcium chloride derived from dolomite chlorination affected the physical properties of magnesium chloride, since they formed an eutectic mixture with a fusion point of 620 °C, which allowed the reaction between liquid magnesium chloride and vitreous silica at 700 °C.

Acknowledgments

The authors wish to thank Universidad Nacional de San Luis (UNSL), Fondo para la Investigación Científica y Tecnológica (FONCyT) and Consejo Nacional de Investigaciones Científicas y Técnicas (CONICET) for financial support.

References

[1] A.I. Avgustinik, Cerámica, Reverté S.A., Barcelona, 1983.
[2] Ch. Nkoumbou, Fr. Villieras, D. Njopwouo, Cl.Y. Ngoune, O. Barres, M. Pelletier, A. Razafitianamaharavo, J. Yvon, Physicochemical properties of talc ore from three deposits of Lamal Pougue area (Yaounde Pan-African Belt Cameroon), in relation to industrial uses, Appl. Clay Sci. 41 (2008) 113–132.
[3] E.A. Takher, T.I. Fedoseeva, V.Y. Kellerman, R. Popilskii, High-strength steatite ceramic with a wide sintered-state range, Glass Ceram. 31 (1974) 108–111.
[4] W.D. Kingery, H.K. Bowen, D.R. Uhlmann, Introduction to Ceramics, Wiley & Sons, New York, 1976.
[5] F. Kharitonov, L.E. Shapiro, A steatite material having a wide sintering range, Glass Ceram. 46 (1989) 162–165.
[6] E. Vela, M. Peiteado, F. García, A.C. Caballero, J.F. Fernández, Sintering behaviour of steatite materials with barium carbonate, Ceram. Int. 33 (2007) 1325–1329.
[7] D. Goeuriot, J.C. Dubois, D. Merle, F. Thevenot, P. Exbrayat, Enstatite based ceramics for machinable prosthesis applications, J. Eur. Ceram. Soc. 18 (1998) 2045–2056.
[8] X. Jin, J. Chang, W. Zhai, K. Lin, Preparation and characterization of clinoenstatite bioceramics, J. Am. Ceram. Soc. 94 (2011) 66–70.
[9] W. Mielcarek, D. Nowak-Woźny, K. Prociów, Correlation between $MgSiO_3$ phases and mechanical durability of steatite ceramics, J. Eur. Ceram. Soc. 24 (2004) 3817–3821.
[10] P.E. Sarquís, M. Gonzalez, Limits of the use of industrial talc—the carbonate effect, Miner. Eng. 11 (1998) 657–660.
[11] M.M. Ahmed, G.A. Ibrahim, M.M.A. Hassan, Improvement of Egyptian talc quality for industrial uses by flotation process and leaching, Int. J. Miner. Process. 83 (2007) 132–145.
[12] R.P. Orosco, M. del C. Ruiz, J.A. González, Purification of talcs by chlorination and leaching, Int. J. Miner. Process. 101 (2011) 116–120.
[13] H.Ş. Soykan, Low-temperature fabrication of steatite ceramics with boron oxide addition, Ceram. Int. 33 (2007) 911–914.
[14] T. Ishii, R. Furuichi, Y. Kobayashi, Thermoanalytical study on the chlorination of magnesium-containing ores: an application of a simple gas-flow differential thermal analysis technique, Thermochim. Acta 9 (1974) 39–53.
[15] F.M. Túnez, J. González, M. del C. Ruiz, Aparato de Laboratorio para Realizar Termogravimetrías en Atmósferas Corrosivas y no Corrosivas, P060100450, 2007.
[16] M. Wesołowski, Thermal decomposition of talc: a review, Thermochim. Acta 78 (1984) 395–421.
[17] D. Sheila, Thermal analysis studies on the decomposition of magnesite, Int. J. Miner. Process. 37 (1993) 73–88.

[18] F. Villieras, J. Yvon, J.M. Cases, P. Donato, F. Lhote, R. Baeza, Development of microporosity in clinochlore upon heating, Clays Clay Miner. 42 (1994) 679–688.
[19] R.M. McIntosh, J.H. Sharp, F.W. Wilburn, The thermal decomposition of dolomite, Thermochim. Acta 165 (1990) 281–296.
[20] J.R. Ward, Kinetics of talc dehydroxylation, Thermochim. Acta 13 (1975) 7–14.
[21] L.A. Hollingbery, T.R. Hull, The thermal decomposition of huntite and hydromagnesite – a review, Thermochim. Acta 509 (2010) 1–11.
[22] N. Kanari, I. Gaballah, E. Allain, A low temperature chlorination–volatilization process for the treatment of chalcopyrite concentrates, Thermochim. Acta 373 (2001) 75–93.
[23] F.C. Gennari, D. Pasquevich, Kinetics of the chlorination of hematite, Thermochim. Acta 284 (1996) 325–339.
[24] J.A. González, M. del C. Ruiz, Bleaching of kaolins and clays by chlorination of iron and titanium, Appl. Clay Sci. 33 (2006) 219–229.
[25] R.P. Orosco, E. Perino, M. del C. Ruiz, J.A. González, A thermogravimetric study of refractory clays chlorination, Int. J. Miner. Process. 98 (2011) 195–201.
[26] N. Kanari, E. Allain, I. Gaballah, Reactions of wüstite and hematite with different chlorinating agents, Thermochim. Acta 335 (1999) 79–86.
[27] C. Robelin, P. Chartrand, A.D. Pelton, ($MgCl_2 + CaCl_2 + MnCl_2 + FeCl_2 + CoCl_2 + NiCl_2$) system, J. Chem. Thermodyn. 36 (2004) 793–808.
[28] HSC Chemistry for Windows Software V. 5.1, 2003. Outokumpu Research, Pori, Finland.